Electrophoresis of pH-Regulated Particles in the Presence of Multiple Ionic Species

Chien Hsu, Duu-Jong Lee, and Jyh-Ping Hsu
Dept. of Chemical Engineering, National Taiwan University, Taipei 10617, Taiwan

Nan Wang
Dept. of Chemical Engineering, National Taiwan University, Taipei 10617, Taiwan

Dept. of Chemistry, College of Chemistry and Chemical Engineering, Huazhong University of Science and Technology, Wuhan 430074, P.R. China

Shiojenn Tseng
Dept. of Mathematics, Tamkang University, Tamsui, Taipei 25137, Taiwan

DOI 10.1002/aic.14276
Published online November 8, 2013 in Wiley Online Library (wileyonlinelibrary.com)

An electrophoresis model taking account of the pH-regulated nature of particles and the presence of multiple ionic species is proposed for arbitrary surface potential and double-layer thickness. It successfully simulated the electrophoretic behavior of Fe_3O_4 nanoparticles in an aqueous NaCl solution with pH adjusted by HCl and NaOH. The estimated zeta potential is compared with those from the conventional models, Smoluchowski's, Hückel's, and Henry's formulas. Due to the violation of the assumption of low and constant surface potential, these formulas yielded appreciable deviations (e.g., 23–30 mV at pH 9). With the surface charge density measured by titration and the zeta potential by electrophoresis, the true surface potential is estimated through a triple-layer model. The estimated true potential is typically 1.5–10 times larger than the zeta potential, implying that using the latter in relevant calculations (e.g., stability and critical coagulation concentration) might yield appreciable deviation. © 2013 American Institute of Chemical Engineers *AIChE J*, 60: 451–458, 2014

Keywords: electrophoresis, pH-regulated particle, multiple ionic species, triple-layer model

Introduction

Being a popular magnetic material, Fe_3O_4 magnetic nanoparticles (MNPs) have attracted significant attention for various applications such as magnetic recording,[1] biological and chemical sensors,[2–4] separation and purification,[5] magnetic resonance imaging,[6] drug delivery,[7] and environmental purification.[8–11] The surface properties of Fe_3O_4 MNPs, especially their charged conditions, are usually tailored to improve their performance. This is because these conditions influence significantly the particle behaviors such as aggregation,[12] interaction with targets (e.g., drugs, proteins, and enzymes),[13–15] and reactivity.[8–11,16] The charged surface arises from the protonation and deprotonation of surface hydroxyl groups on the oxide. Fe_3O_4 MNPs have an acid dissociation constant K_a of $10^{-6.66}\sim10^{-9.1}$,[17–19] basic dissociation constant K_b of $10^{5.96}\sim10^{6.6}$,[17–19] and the point of zero charge (PZC) of pH 3.8–9.9.[20] These parameters are dependent on the preparation processes of Fe_3O_4 and the dispersion conditions. Like other colloidal particles, the charged conditions of Fe_3O_4 MNPs are usually characterized by zeta potential,[13,21,22] the electric potential of a charged particle on the inner boundary of its diffuse layer. The zeta potential of a particle is commonly adopted to represent its surface potential, which is not experimentally measurable. Experimentally, electrophoresis is first conducted to obtain mobility, and then a mobility-potential relationship applied to evaluate the corresponding zeta potential.

Assuming a low (<25.4 mV) constant surface (zeta) potential and infinitely thin double layer, Smoluchowski[23] showed that the electrophoretic mobility of an isolated, rigid particle μ_E can be expressed as $\mu_E=\varepsilon\zeta_p/\eta$ with ε, ζ_P, and η being the permittivity of the liquid phase, the zeta potential, and the fluid viscosity, respectively. The counterpart of infinitely thick double layer was derived by Hückel[24] as $\mu_E=(2/3)(\varepsilon\zeta_p/\eta)$. These two limiting cases were later generalized to an arbitrary double-layer thickness by Henry[25] as $\mu_E=2\varepsilon\zeta_P f(\kappa a)/(3\eta)$ with $f(\kappa a)$ being the Henry's function, which increases monotonically from 1 as $\kappa a \rightarrow 0$ to 1.5 as $\kappa a \rightarrow \infty$, with κa being the double-layer thickness. Henry's formula is the foundation of many electrophoresis-based zeta potential instruments. In addition to low surface potential, the derivation of this formula also assumed that the effect of double-layer polarization/relaxation is negligible and the

Additional Supporting Information may be found in the online version of this article.

Correspondence concerning this article should be addressed to J. -P. Hsu at jphsu@ntu.edu.tw, and S. Tseng at topology@mail.tku.edu.tw.

total potential is the sum of the potential coming from the particle and that from the applied electric field.

Unfortunately, the above assumptions are often violated in practice. For instance, a surface (zeta) potential that is much higher than 25.4 mV is not uncommon for many colloidal particles under typical conditions. As pointed out by Hsu et al.,[26–28] the polarization of double layer should be considered when its thickness is comparable to the particle size and the surface potential is not low. For many metal oxide particles, the assumption of constant surface potential is unrealistic because, due to surface reactions, the charged conditions of their surface depend upon factors such as pH and bulk salt concentration. This also raises the problem that the particle size might vary with those factors because a reduction in the electric repulsion between two particles might lead to their aggregation. Furthermore, because the pH of a dispersion is often adjusted with acid or basic, the presence of multiple ionic species in the liquid phase coming from background salt and introduced acid/base should be considered. This factor is almost always overlooked in previous theoretical analyses. The above-mentioned violations imply that the zeta potential estimated from Smoluchowski's, Hückel's, and Henry's formulas can be unreliable and using a more rigorous model is both desirable and necessary. O'Brien and White[29] extended these analyses to the case of the electrophoresis of a rigid sphere at arbitrary levels of surface potential and double-layer thickness. The effect of double-layer polarization considered yields complicated and interesting results in particle mobility. However, their model needs further extension for two reasons. First, the surface of particles such as metal oxides is charge regulated due to surface reactions so that its surface potential varies with liquid conditions instead of maintaining at a constant level. Second, the liquid phase contains multiple ionic species rather than binary electrolyte only, implying that the thickness of double layer is underestimated in the latter, especially when the solution pH deviates appreciably from the isoelectric point (IEP) of the dispersed particles.

In this study, a mobility model taking account of the pH-regulated nature of a particle, the presence of multiple ionic species, and the effect of double-layer polarization is proposed for the case of arbitrary potential and double-layer thickness. The true surface potential is also estimated based on a triple-layer model[30,31] and the density of the dissociable functional groups on the particle surface obtained from titration. This model was also adopted by Sonnefeld et al.[32] to estimate the double-layer parameters of spherical silica from titration data and electrokinetic sonic amplitude measurements based on binary electrolyte.

Theory

Figure 1 illustrates schematically the problem considered: the electrophoresis of a rigid sphere of radius a and surface Ω_p driven by an applied uniform electric field $\mathbf{E}$ of strength E. r, θ, φ are the spherical coordinates with the origin coincides with the particle center. For convenience, a z axis is also defined, and $\mathbf{E}$ is the z direction. The particle velocity $\mathbf{U}_p$ with magnitude U_p is also in that direction.

We assume that the following reactions occur on the particle surface

$$\equiv \mathrm{M{-}OH_2^+} \iff \equiv \mathrm{M{-}OH} + \mathrm{H^+} \tag{1}$$

$$\equiv \mathrm{M{-}OH} \iff \equiv \mathrm{M{-}O^-} + \mathrm{H^+} \tag{2}$$

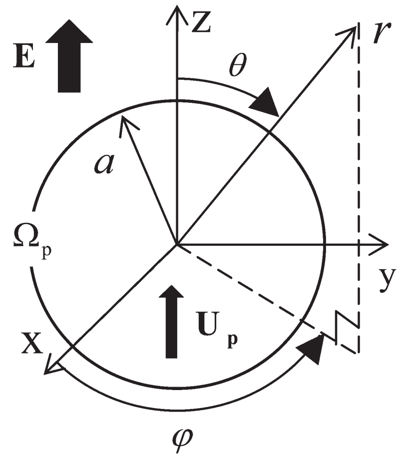

Figure 1. Electrophoresis of a rigid spherical particle of radius *a*, velocity $\mathbf{U_p}$, and surface Ω_p driven by an applied uniform electric field E; *r*, *θ*, *φ* are the spherical coordinates with the origin coincides with the particle center; both $\mathbf{U_p}$ and E are in the *z* direction.

where $\equiv \mathrm{M{-}OH}$ denotes the functional group. These expressions suggest that the particle surface is zwitterionic and pH regulated. Let $K_b = N_{\equiv \mathrm{M-OH_2^+}} / N_{\equiv \mathrm{M-OH}} [\mathrm{H^+}]$ and $K_a = N_{\equiv \mathrm{M-O^-}} [\mathrm{H^+}] / N_{\equiv \mathrm{M-OH}}$ be the corresponding equilibrium constant with $N_{\equiv \mathrm{M-OH_2^+}}$, $N_{\equiv \mathrm{M-OH}}$, $N_{\equiv \mathrm{M-O^-}}$, and $[\mathrm{H^+}]$ being the surface densities of $\equiv \mathrm{M{-}OH_2^+}$, $\equiv \mathrm{M{-}OH}$, $\equiv \mathrm{M{-}O^-}$, and the surface concentration of $\mathrm{H^+}$, respectively. Let $N_{\mathrm{total}} = N_{\equiv \mathrm{M-O^-}} + N_{\equiv \mathrm{M-OH}} + N_{\equiv \mathrm{M-OH_2^+}}$ be the total surface density of $\equiv \mathrm{M{-}OH}$.

Suppose that the liquid phase is an incompressible Newtonian fluid, the flow field is in the creeping flow region, and the system is at a pseudosteady state. Then the present problem can be described by[33]

$$\nabla^2 \phi = -\frac{\rho}{\varepsilon} = -\sum_{j=1}^{N} \frac{z_j e n_j}{\varepsilon} \tag{3}$$

$$\mathbf{f}_j = -D_j \left(\nabla n_j + \frac{z_j e}{k_B T} n_j \nabla \phi \right) + n_j (\mathbf{u} - \mathbf{u}_p) \tag{4}$$

$$\nabla \cdot \mathbf{f}_j = 0 \tag{5}$$

$$-\nabla p + \eta \nabla^2 \mathbf{u} - \rho \nabla \phi = \mathbf{0} \tag{6}$$

$$\nabla \cdot \mathbf{u} = 0 \tag{7}$$

Here, ϕ, ρ, and e are the electrical potential (V), the space density of mobile ions (Coul/m^2), and the elementary charge (Coul), respectively; k_B, T, $\mathbf{u}$, and p are Boltzmann constant (J/K), the absolute temperature (K), the fluid velocity (m/s), and the pressure (Pa), respectively. z_j, n_j, $\mathbf{f}_j$, and D_j, are the valence, the number concentration (1/m^3), the flux (1/s/m^2), and the diffusivity (m^2/s) of ionic species j, respectively, $j = 1,2,\ldots,N$, with N being the number of kinds of ionic species in the liquid phase.

We assume that the electric field established by the particle is much stronger than $\mathbf{E}$. This is usually satisfied because the lower limit of the particle surface potential is on the order of 25 mV and the Debye length ranges normally from 10 to 100 nm so that the strength of the electric field established by the particle ranges form 250 to 2500 kV/m, which is much higher than that of the applied electric field. Therefore, instead of solving Eqs. 3–7 directly, a perturbation approach is adopted, where each dependent variable is decomposed into an equilibrium component and a perturbed component.[29] The equilibrium and perturbed components of a variable are its value when **E** is absent and that when **E** is applied, respectively. Using a prefix δ and a subscript e to denote a perturbed component and an equilibrium component, respectively, it can be shown that Eqs. 8–13 yield,[34,35]

$$\nabla^2\phi_e=-\frac{\kappa^2\zeta_a}{\sum_{j=1}^{N}\frac{z_j^2 n_{j0}}{z_1^2 n_{10}}}\sum_{j=1}^{N}\frac{z_j n_{j0}}{z_1 n_{10}}\exp\left(-\frac{z_j}{z_1}\frac{\phi_e}{\zeta_a}\right) \tag{8}$$

$$\nabla^2\delta\phi=\frac{\kappa^2}{\sum_{j=1}^{N}\frac{z_j^2 n_{j0}}{z_1^2 n_{10}}}\sum_{j=1}^{N}\frac{z_j^2 n_{j0}}{z_1^2 n_{10}}(\delta\phi+g_j)\exp\left(-\frac{z_j}{z_1}\frac{\phi_e}{\zeta_a}\right) \tag{9}$$

$$\nabla^2 g_j=\frac{z_j}{z_1}\frac{1}{\zeta_a}\nabla\phi_e\cdot\nabla g_j+\frac{1}{D_j}(\delta\mathbf{u}-\mathbf{U}_\mathrm{p})\cdot\nabla\phi_e \tag{10}$$

$$\eta\nabla^2\delta\mathbf{u}-\nabla\delta p+\varepsilon\nabla^2\phi_e\nabla\delta\phi+\varepsilon\nabla^2\delta\phi\nabla\phi_e=\mathbf{0} \tag{11}$$

$$\nabla\cdot\delta\mathbf{u}=0 \tag{12}$$

$$n_j=n_{j0}\exp\left(-\frac{z_j}{z_1}\frac{\phi_e}{\zeta_a}\right)\left(1-\frac{z_j}{z_1}\frac{(\delta\phi+g_j)}{\zeta_a}\right),j=1,2,...,N \tag{13}$$

Here, $\kappa=[\sum_{j=1}^{N}n_{j0}(ez_j)^2/\varepsilon k_B T]^{1/2}$ and $\zeta_a=k_BT/z_1e$ are the reciprocal Debye length and the thermal potential, respectively; subscript 1 denotes a reference ionic species; n_{j0} is the bulk number concentration (1/m^3) of ionic species j; g_j is a perturbed potential (V) simulating the polarization of particle's double layer.

Suppose that the particle surface is nonconductive, impenetrable, and nonslip, and the electric and flow fields far away from it are uninfluenced by its presence. These yield the following boundary conditions

$$\mathbf{n}\cdot\nabla\phi_e=0 \text{ as } \mathrm{r}\rightarrow\infty \tag{14}$$

$$\mathbf{n}\cdot\nabla\delta\phi=\mathrm{E} \text{ as } \mathrm{r}\rightarrow\infty \tag{15}$$

$$g_j=-\delta\phi \text{ as } \mathrm{r}\rightarrow\infty \tag{16}$$

$$\mathbf{n}\cdot\nabla\delta\mathrm{u}=0 \text{ as } \mathrm{r}\rightarrow\infty \tag{17}$$

$$\mathbf{n}\cdot\nabla\delta\phi=0 \text{ as } \mathrm{r}\rightarrow\infty \text{ or on } \Omega_\mathrm{p} \tag{18}$$

$$\mathbf{n}\cdot\nabla g_j=0 \text{ as } \mathrm{r}\rightarrow\infty \text{ or on } \Omega_\mathrm{p} \tag{19}$$

$$\delta\mathbf{u}=\mathbf{0} \text{ as } \mathrm{r}\rightarrow\infty \tag{20}$$

$$\mathbf{n}\cdot\nabla\phi_e=-\frac{\sigma_\mathrm{s}}{\varepsilon}=\frac{FN_\mathrm{total}}{\varepsilon}\left(\frac{K_a-K_b([\mathrm{H}^+]_0\exp(-\frac{\phi_e}{\zeta_a}))^2}{K_a+[\mathrm{H}^+]_0\exp(-\frac{\phi_e}{\zeta_a})+K_b([\mathrm{H}^+]_0\exp(-\frac{\phi_e}{\zeta_a}))^2}\right)\text{ on }\Omega_\mathrm{p} \tag{21}$$

$$\delta\mathbf{u}=U_p\mathbf{e}_\mathrm{r}\cos\theta \text{ on } \Omega_\mathrm{p} \tag{22}$$

Here, σ_s, F, $[\mathrm{H}^+]_0$, $\mathbf{e}_\mathrm{r}$, and $\mathbf{n}$ are the surface charge density (Coul/m^2 or mol/m^2), Faraday constant (Coul/mol), the bulk molar concentration (mol/m^3) of H^+, the unit vector in the r direction, and the unit outer normal vector. Note that $\delta p=0$ as $\mathrm{r}\rightarrow\infty$ and $\mathbf{v}_\mathrm{e}=\mathbf{0}$ because no pressure gradient is imposed and the particle is at rest when **E** is absent.

The governing equations and the associated boundary conditions are solved numerically by FlexPDE (PDE Solutions, Spokane Valley, WA) through a trial-and-error procedure.[36] The electrophoretic mobility of the particle, μ_E, is defined as $\mu_E=U_p/E$.

To examine the applicability of the present model, we consider an aqueous NaCl dispersion of Fe_3O_4 particles with pH adjusted by HCl and NaOH, implying that four kinds of ionic species need be considered: Na^+, H^+, OH^-, and Cl^-. The following values apply at 25°C:[37–40] $\varepsilon=6.94\times10^{-10}$F/m, $\eta=8.96\times10^{-4}$kg/m/s, $D_{\mathrm{Na}^+}=1.33\times10^{-9}$, $D_{\mathrm{H}^+}=9.31\times10^{-9}$, $D_{\mathrm{OH}^-}=5.3\times10^{-9}$, $D_{\mathrm{Cl}^-}=2\times10^{-9}$, and $K_w=14$. Based on the reported values for K_a and K_b, $10^{-6.66}\sim10^{-9.1}$ and $10^{5.96}\sim10^{6.6}$, respectively,[17–19] we assume $K_a=10^{-8.5}$ and $K_b=10^6$, and $K_\mathrm{w}=10^{-14}$.

Experimental

Materials

Ferrous sulfate heptahydrate ($FeSO_4$•$7H_2O$, 99.0%), ferric trichloride hexahydrate ($FeCl_3$•$6H_2O$, 99.0%), ammonium hydroxide (NH_4OH, 28%), and hydrogen chloride (HCl, 35%) (Showa Chemical Industry, Japan), and NaCl (J.T. Baker-Mallinckrodt, 101.5%) of reagent grade were used. Potassium hydrogen phthalate ($C_8H_5KO_4$, 99.8%) were purchased from Sinopharm Chemical Reagent (Shanghai, China). The N_2 gas with high purity was obtained from Air Products, Taiwan. Deionized water with a resistivity of 18.2 MΩ cm was used.

Preparation and characterization of Fe_3O_4 MNPs

Fe_3O_4 MNPs were prepared by an advanced reverse coprecipitation method assisted by ultrasound irradiation.[41] The Fe_3O_4 MNPs obtained were water washed to neutral pH, redispersed in water, and then stored at 5°C under anoxic atmosphere (referred to as the stock solutions with the mass concentration of 5.6 and 22.1 g/L in electrophoresis measurements and titration experiments, respectively, and the Fe^{2+}/Fe^{3+} molar ratio of 1:2). As reported in our previous work, Fe_3O_4 MNPs were roughly spherical with an averaged primary particle diameter of about 40 nm, and high crystallinity.[41,42] The Brunauer–Emmett–Teller (BET) surface area was determined with low-temperature N_2 adsorption-desorption experiments by Micromeritics ASAP 2020. Before BET measurements, the Fe_3O_4 MNPs were first collected by magnetic separation and vacuum dried at 50°C for 1 h, and then dehydrated at 200° C for 6 h. The measured BET surface area was about 80 m^2/g. The hydrodynamic size was characterized by ZetaSizer Nano ZS (Malvern Instruments, UK) at 633 nm red laser, based on dynamic light scattering (DLS). Dispersions were ultrasonicated for 2 min before size measurements. The pH-dependent surface charge of Fe_3O_4 MNPs was determined by acid-base titration with NaOH or HCl standard on a ZDJ-4A automatic titrator equipped with E-201-C-65 pH electrode (Shanghai Precision & Scientific Instruments, China). In the blank experiment, a reference solution was obtained by separating Fe_3O_4 MNPs with a centrifugation at 14, 000 rpm for 15 min and the subsequent filtration with a 0.22 μm filter membrane, and it was titrated by the same procedure used in the colloidal suspension. The titration details were shown in Supporting Information, Section S1. Based on the titration curve, the surface

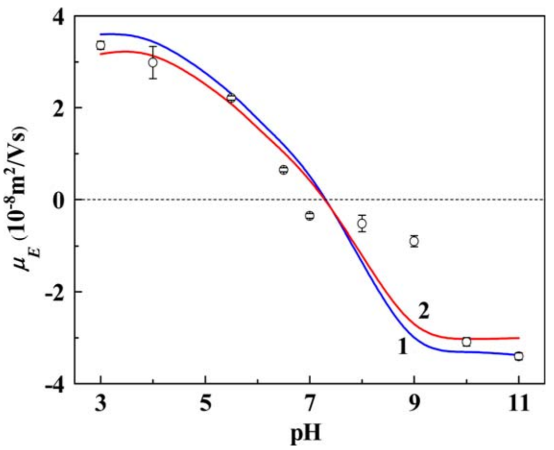

Figure 2. Variation of electrophoretic mobility μ_E with pH at different values of the apparent total density of functional groups, $N_{total,ap}$.

Discrete symbols with error bars: experimental data; curves: theoretical results. Curve 1, $N_{total,ap} = 0.06$ no./nm^2; curve 2, $N_{total,ap} = 0.05$ no./nm^2. [Color figure can be viewed in the online issue, which is available at wileyonlinelibrary.com.]

charge density (σ_s, mol/m^2 or Coul/m^2) of Fe_3O_4 MNPs can be expressed as

$$\sigma_s = \frac{(c_{HCl} + c_{OH^-} - c_{H^+})(V_{HCl}^S - V_{HCl}^B)}{mS} \tag{23}$$

where c_{HCl} (mol/L) is the molar concentration of acid as the titrant, V_{HCl}^S (L) and V_{HCl}^B (L) are the volume of the acid added to the Fe_3O_4 suspensions and reference blank solution, respectively; m (g) and S (m^2/g) are the weight and the BET surface area of Fe_3O_4 MNPs, respectively.

Electrophoresis measurements

The electrophoretic mobility of Fe_3O_4 MNPs was also measured by ZetaSizer Nano ZS with a laser Doppler electrophoresis technique at 25°C. Unless otherwise specified, N_2-saturated electrolyte solution containing 1 mmol/L NaCl solution was used to disperse Fe_3O_4 MNPs. The solution pH, which ranged from 3 to 11, was adjusted by either 0.1 mol/L HCl or 0.1 mol/L NaOH. After the introduction of Fe_3O_4 MNPs into the electrolyte solution at a given pH, the dispersion was ultrasonicated for 1 min, and then rapidly transferred into a folded capillary cell with two caps. The atmosphere was protected with nitrogen purging before transferring sample to the capillary cell. Because previous work has demonstrated that the electrophoretic mobility was almost constant after 2 min in Supporting Information Figure S3,[42] we assumed that equilibration is reached at this time. The ZetaSizer Nano ZS was calibrated by a carboxy-modified polystyrene latex standard sample ($\zeta = -68 \pm 6.8$ mV at 25°C) before each set of measurements. Each measurement had three replicates, and the averaged mobility with error bars was recorded.

Results and Discussion

Mobility

Figure 2 summarizes the variation in the electrophoretic mobility μ_E with pH. In addition to the experimental data, the values predicted by the present model for two different values of N_{total} are also presented. It shows that the experimental μ_E is positive for pH lower than about 7, and becomes negative once it exceeds pH 7. For positive values of μ_E, μ_E decreases with increasing pH, and for negative values of μ_E, $|\mu_E|$ increases with increasing pH. This is because μ_E has the same sign as the surface potential, and the more the deviation of pH from the IEP (where $\mu_E = 0$) the more complete the dissociation/association of $\equiv$Fe$-$OH , yielding a higher surface charge density and, therefore, a larger $|\mu_E|$. The theoretical calculation of μ_E involves the particle radius a, the equilibrium constants K_a and K_b, and the total number density of the surface hydroxyl site N_{total}. Note that, due to the possible aggregation of particles, a might vary with pH, as is verified in Table 1 and Supporting Information Table S1, where the measured hydrodynamic sizes of Fe_3O_4 MNPs are illustrated. K_a and K_b are chosen as $10^{-8.5}$ and 10^6, respectively.[17–19] Using these values, the calculated μ_E can fit well the experimental data for an N_{total} (no./nm^2) in the range [0.05,0.06]. As such an N_{total} is estimated from electrophoretic measurements, it is defined as the apparent N_{total}, $N_{total,ap}$, for convenience. Note that $N_{total,ap}$ is much lower than that estimated from previous titration experiments (2.2–3.1 no./nm^2),[16,43] as ours ($N_{total} = 2.1$ no./nm^2). Similar results were also observed for SiO_2 particles,[44,45] where N_{total} can be 15 times larger than $N_{total,ap}$. Figure 2 also showed that the relative deviation of μ_E (experiment) from μ_E (theory) near pH 7 is larger than those at other pH values, but most calculated values of μ_E based on a proper $N_{total,ap}$ agree well with the experimental data. As will be shown later, this is because the potential is low near IEP, yielding a small electrostatic repulsion between Fe_3O_4 MNPs, and therefore, appreciable particle aggregation, making accurate measurements in hydrodynamic radius and mobility

Table 1. Values of κa in the Zeta Potential Measurements for Fe_3O_4 NPs (10 mg/L) in 1 mmol/L NaCl (k =1. 04 × 10^8 m^{-1}), Where the Solution pH is Adjusted by 0.1 mol/L HCl and NaOH

pH	a (nm)	ka	$f(\kappa a)$	[H$^+$] (mol/L)	κ' (10^8 m^{-1})[a]	κ'a
3	44.6	4.64	1.14	1E-3	1.47	6.56
4	46.2	4.80	1.15	1E-4	1.09	5.04
5.5	53.0	5.51	1.17	3.2E-6	1.04	5.51
6	70.6	7.34	1.20	1E-6	1.04	7.34
7	653.0	67.91	1.45	1E-7	1.04	67.91
8	279.2	29.04	1.38	1E-8	1.04	29.04
9	194.2	20.20	1.34	1E-9	1.04	20.20
10	46.6	4.85	1.15	1E-10	1.09	5.08
11	38.7	4.02	1.13	1E-11	1.47	5.69

[a]κ' denotes the real reciprocal Debye length taking account of the presence of multiple ionic species coming from the background NaCl and the introduced acid/base.

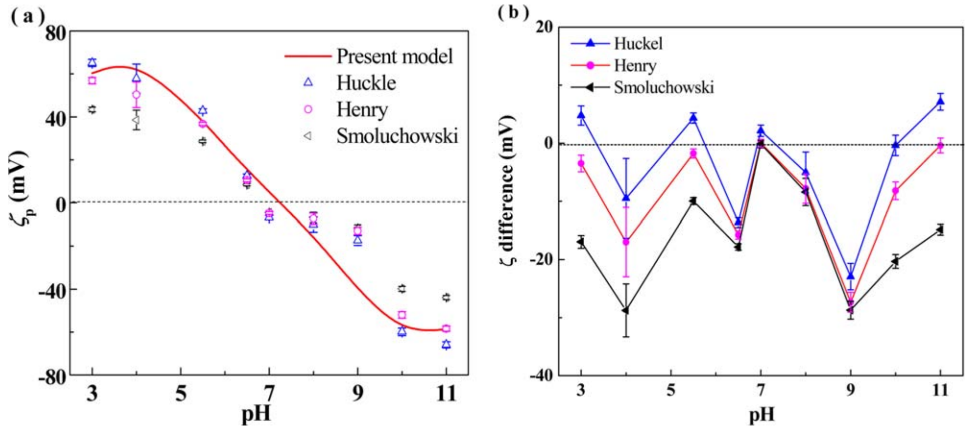

Figure 3. Variation of zeta potential ζ, (a), and difference in ζ, ζ(classic formula)- ζ(present model), (b), with pH.

In (a), discrete symbols with error bars denote ζcalculated from the experimental electrophoresis data with classic formula; curve denotes the present theoretical result at $N_{total,ap} = [(0.05 + 0.06)/2]$ no./nm^2. [Color figure can be viewed in the online issue, which is available at wileyonlinelibrary.com.]

nontrivial. These results suggest that the performance of our electrophoretic model is satisfactory.

As can be seen in Table 1, the particle size a near IEP is considerably larger than that at other pH values, implying the occurrence of particle aggregation. This suggests that the scaled double-layer thickness, κa, varies with both the bulk ionic concentrations and pH. Therefore, considering the presence of all the ionic species (Na^+, H^+, Cl^-, and OH^-) is necessary. Note that at pH 3, the thickness of double layer when all the multiple ionic species are considered (Na^+, H^+, Cl^-, and OH^-), $\kappa' a$, is 1.41 folds of that when only Na^+ and Cl^- are considered, κa.

Zeta potential

The variation in the measured zeta potential ζ (i.e., ϕ_e in Eq. 21) with pH is presented in Figure 3a, where both Smoluchowski's and Hückel's formulas provided by the instrument manufacturer are selected to transform μ_E to ζ. For comparison, Henry's formula

$$\mu_E = \frac{2\varepsilon\zeta}{3\eta} f(\kappa a) \tag{24}$$

$$f(\kappa a) = 1.5 - \frac{0.5}{1 + 0.07234(\kappa a)^{1.129}} \tag{25}$$

is also adopted to transform μ_E to ζ. Figure 3a reveals that the $|\zeta|$ based on Smoluchowski's formula is smaller than that based on Hückel's formula. This is because a factor of 1.5 is assumed for $f(\kappa a)$ in the former and 1.0 in the latter. The estimated IEP of Fe_3O_4 MNPs is about pH 7, which is in good agreement with the literature value.[20]

As seen in Figure 3a, both the present model and the classic formulas are capable of describing successfully the qualitative behavior of the experimental data. However, the accuracy of the estimated zeta potential from experimentally measured electrophoretic velocity depends upon the choice of a velocity-zeta potential formula. As the main assumptions of the classic formulas (low and constant potential, binary electrolytes, etc.) are usually violated and our model is closer to reality, it is chosen as the basis for comparison. Figure 3b reveals that both Smoluchowski's and Henry's formulas underestimate ζ, whereas Hückel's formula may overestimate ζ. The difference between these formulas and the present model can be appreciable, in general. The deviations of Smoluchowski's and Hückel's formulas come from that $\kappa a \to \infty$ (infinitely thin double layer) and $\kappa a \to 0$ (infinitely thick double layer) are assumed, respectively, so that $f(\kappa a)$ is 1.5 in the former and 1.0 in the latter. However, as seen in Table 1, κa varies from 4 to 68, implying that $f(\kappa a)$ is between 1 and 1.5, and therefore, ζ might be underestimated (overestimated) by Smoluchowski's (Hückel's) formula. Note that the assumptions of Henry's formula (i.e., low constant surface potential, only Na^+ and Cl^- are considered, double-layer polarization negligible) are suitable near IEP. However, it might result in considerable derivation in ζ as pH deviates from IEP. For example, the deviations are about 15 and 30 mV at pH 4 and 9, respectively. For other systems, where the potential is high, the deviation of Henry's formula can be more serious. It is interesting to see that our model predicts the presence of a positive local maximum in ζ near pH 4 and a negative local minimum near pH 10, but the classic models are unable to predict these. The presence of those local extrema can be explained by the variation in the double-layer thickness with pH presented in Table 1, which shows that $\kappa' a$ has a local minimum as pH decreases (increases) from IEP to pH 3 (11), but κa decreases monotonically. The presence of the negative local minimum in ζ as pH varies was also found by Hsu and Tai[46] in a theoretical study of the electrophoresis of SiO_2. Because IEP is pH 2 in their case, the positive local maximum in ζ was not seen in their numerical simulation, where pH >3.

Surface charge density

Figure 4 shows the variation of the surface charge density of Fe_3O_4 MNPs, σ_S, with solution pH at 1 mmol/L NaCl. For comparison, the corresponding value based on electrophoresis, σ_{app}, is also presented. As can be seen, both σ_S and σ_{app} vary roughly linearly with pH; $\sigma_S > 0$ ($\sigma_{app} > 0$) for pH <7.0, and $\sigma_S < 0$ ($\sigma_{app} < 0$) for pH >7, implying that the PZC of Fe_3O_4 MNPs is about pH 7.0, which is consistent with the pH_{IEP} based on electrophoresis. This strong dependence of σ_S (σ_{app}) on pH can be explained by the protonation/deprotonation of the amphoteric surface groups of Fe_3O_4 MNPs (Eqs. 1 and 2). Moreover, as expected, σ_S is much larger than σ_{app}, which is consistent with the results of Missana and Adell.[47]

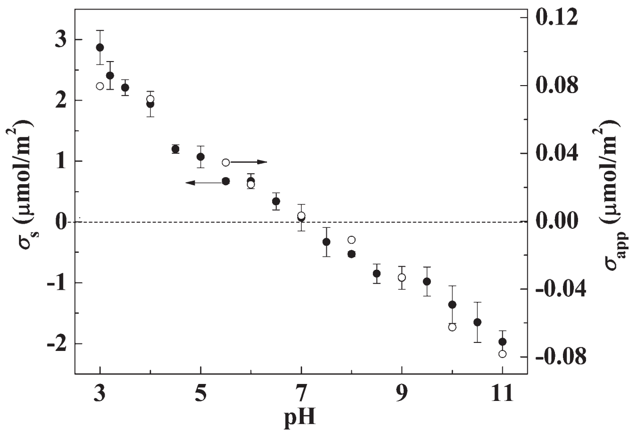

Figure 4. Variations of the surface charge density of Fe_3O_4 NPs based on titration and electrophoresis, σ_S (solid symbols with error bar) and σ_{app} (open symbols), respectively, with solution pH at 1 mmol/L NaCl and 25°C.

Estimation the true surface potential

The zeta potential ζ estimated from electrophoresis data is not the true surface potential ϕ_S; the latter should be used, for example, in assessing the stability (or critical coagulation concentration) of a colloidal dispersion. Based on the surface charge density, σ_S, estimated from titration, ϕ_S can be estimated by a model describing the double-layer structure. To this end, we adopt the triple-layer model[30] illustrated in Figure 5.

Let σ_{app}, ϕ_{IHP}, and ϕ_{OHP} $(=\zeta)$ be the apparent charge density obtained from Eq. 21, the potential on the inner Helmholtz plane (IHP), and that on the outer Helmholtz plane (OHP), respectively. Then ϕ_S can be obtained by solving[30]

$$\phi_{OHP}=\phi_S-\frac{d_1\sigma_S}{\varepsilon_1\varepsilon_0}-\frac{d_2\sigma_{app}}{\varepsilon_2\varepsilon_0}=\phi_S+d_1s_1+d_2s_2 \tag{26}$$

or

$$\phi_S=\phi_{OHP}-d_1s_1-d_2s_2 \tag{26a}$$

Here, $s_1=-\sigma_S/\varepsilon_1\varepsilon_0$, $s_2=-\sigma_{app}/\varepsilon_2\varepsilon_0$, ε_0, ε_1, and ε_2, are the permittivity of a vacuum, the relative permittivity of the phase between the particle surface and IHP, and that between IHP and OHP, respectively. d_1 and d_2 are the bare radius of counterions and the distance between IHP and OHP, respectively. Typically, d_2 ranges from 1 to 3 diameters of hydrated ions.[48] Because multiple ionic species are present, d_1 is defined as the averaged bare radius of all the types of counterions present. For pH < IEP, the counterions are Cl^- and OH^-, and coions are Na^+ and H^+; for pH > IEP, the counterions are Na^+ and H^+, and coions are Cl^- and OH^-. The bare radii of Na^+, H^+, Cl^-, and OH^- are 0.117, 0.115, 0.164, and 0.133 nm, respectively.[48]

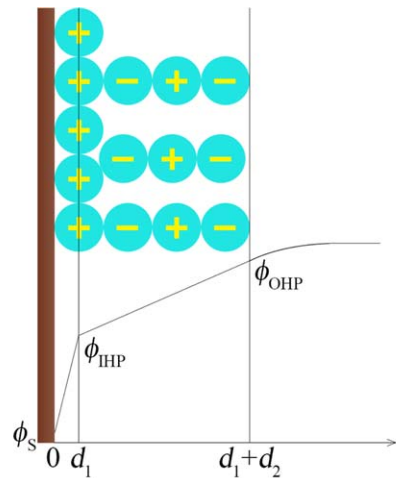

Figure 5. Triple-layer model[26] showing the structure of the electric double layer, where ϕ_S and σ_S are the actual surface potential and surface charge density, respectively; ϕ_{IHP} and ϕ_{OHP} are the potential on the IHP and that on the OHP, respectively; d_1 and d_2 are the distance between the particle surface and IHP and that between IHP and OHP, respectively.

[Color figure can be viewed in the online issue, which is available at wileyonlinelibrary.com.]

For convenience, we use the diameter of hydrated H^+, d_{H+}, as a base to describe d_2. Referring to Figure 5, we define the minimum value of d_2, $d_2(\min)=d_{H+}$, and the maximum value of d_2, $d_2(\max)=4d_{H+}$ which is about the sum of two hydrated diameter of Cl^-, one hydrated diameter of Na^+, and one bare radius of H^+. Table 2 summarizes the variations of σ_S, ε_1, ϕ_{OHP}, $-s_2d_2(\max)$, $-s_1d_1$, ϕ_{Smax}, $-s_2d_2(\min)$, and ϕ_{Smin} with pH, where ϕ_{OHP} is the zeta potential estimated by electrophoresis measurement. ϕ_{Smax} (ϕ_{Smin}) is the value of ϕ_S when $d_2(\max)$ ($d_2(\min)$) is used. Note that ε_1 varies with σ_S.[30] The hydrated radius of Cl^-, Na^+, and H^+ are 0.332, 0.358, and 0.28 nm, respectively.[48] Table 2 reveals that, except for pH near IEP, $|s_1d_1|$ is much larger than $|s_2d_2(\max)|$ or $|\phi_{OHP}|$, implying that $-s_1d_1$ is much more important than the other two terms on the right-hand side of Eq. 26a. In addition, both ϕ_{Smax} and ϕ_{Smin} are about 10 times larger than ϕ_{OHP} at pH 3, and one to two times larger than ϕ_{OHP} at other pHs. This can be explained by that ε_1 decreases drastically as pH varies from 4 to 3. For $\sigma_s<10$ μC/cm², ε_1 is nearly constant as σ_s varies, but

Table 2. Variations of σ_S(μC/cm²), ε_1, ϕ_{OHP}(mV), $-s_2d_2(\max)$(mV), $-s_1d_1$(mV), ϕ_{Smax}(mV), $-s_2d_2(\min)$(mV), and ϕ_{Smin}(mV) with pH

pH	σ_s	$\varepsilon_1(-)$	ϕ_{OHP}	$-s_2d_2(\max)$	$-s_1d_1$	ϕ_{Smax}	$-s_2d_2(\min)$	ϕ_{Smin}
3	27.74	9.1	55.5	24.81	511.29	591.6	6.20	573
4	18.71	40	62.9	22.43	78.45	163.8	5.61	147
5.5	6.45	75.9	36.5	10.75	14.26	61.5	2.69	53.4
6	6.45	75.9	24.6	6.76	14.26	45.7	1.69	40.6
7	0.65	77	4.4	1.05	1.41	6.8	0.26	6
8	−5.16	75.9	−14.1	−3.46	−8.91	−26.5	−0.86	−23.9
9	−8.88	74.4	−38.3	−10.32	−15.63	−64.2	−2.58	−56.5
10	−13.15	65.5	−56.8	−19.44	−26.30	−102.5	−4.86	−87.9
11	−18.99	40	−54.2	−24.40	−62.19	−140.8	−6.10	−122.5

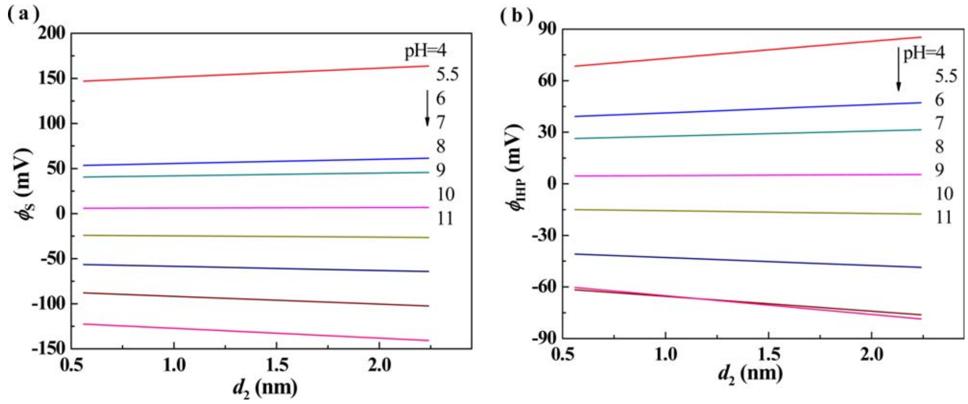

Figure 6. Variations of ϕ_S, (a), and ϕ_{IHP}, (b), with d_2 at various levels of pH.

[Color figure can be viewed in the online issue, which is available at wileyonlinelibrary.com.]

decreases drastically with increasing σ_s for $10 < \sigma_s < 30$ μC/cm^2.[30] Because $\sigma_s/\varepsilon_1(\text{pH}=3) \cong 6.5\sigma_s/\varepsilon_1(\text{pH}=4)$, $-s_1d_1(\text{pH}=3) \cong -6.5s_1d_1(\text{pH}=4)$, making an appreciable difference between $\phi_{\text{Smax}}(\text{pH}=3)$ and $\phi_{\text{Smax}}(\text{pH}=4)$, and ϕ_{Smin} (pH = 3) and ϕ_{Smin} (pH = 4). We conclude that the difference between the values of ϕ_{Smax} (ϕ_{Smin}) at different pH levels comes mainly from the difference in s_1d_1, rather than that in $s_2d_2(\text{max})$ ($s_2d_2(\text{min})$) or in ϕ_{OHP}.

Figure 6a further illustrates the role of $-s_1d_1$, where ϕ_S is seen to be almost independent of d_2, except when pH deviates appreciable from IEP (e.g., pH 4 and 10). As seen in Figure 6b, if $-s_1d_1$ is excluded from the right-hand side of Eq. 26a, the general trend of ϕ_{IHP} is almost the same as that of ϕ_S in Figure 6a. Note that the curves of pH 10 and 11 in Figure 6b almost coincide, which is not the case in Figure 6a. This also verifies that $-s_1d_1$ dominates.

Conclusions

The surface properties of Fe_3O_4 MNPs in an aqueous NaCl solution with pH adjusted by HCl and NaOH are characterized by both electrophoresis and titration. An electrophoresis model taking account of the pH-regulated nature of a particle, the presence of multiple ionic species, and the effect of double-layer polarization was proposed to evaluate the electrophoretic mobility of the particle. The measured mobility was used to estimate the corresponding zeta potential by the present model and the three classic mobility-potential formulas: Smoluchowski, Hückel, and Henry, the former two are usually adopted by conventional zeta potential instrumentation. We show that, depending upon the solution pH, these classic formulas might yield appreciable deviation. For example, it is about 10–30 mV at pH 4 and 23–30 mV at pH 9. Our model also predicts that, due to the variation of the double-layer thickness with pH, the zeta potential has a positive local maximum near pH 4 and a negative local minimum near pH 10; the classic models are unable to predict these. Using the results of titration, the true surface potential is estimated by a triple-layer model. Depending upon pH, the level of the true surface potential can be several times that of zeta potential. For example, ϕ_{Smax} (ϕ_{Smin}) is 10.7 (10.3) times of ϕ_{OHP} (i.e., zeta potential) at pH 3. This implies that if zeta potential is used to estimate parameters such as the number density of surface sites and the stability (or critical coagulation concentration) of a dispersion, the obtained results will underestimate appreciably the true values. It should be pointed out that the physical properties of a particle (e.g., equilibrium dissociation/association constant) and the surrounding liquid medium (e.g., permittivity, viscosity, and ionic diffusivity) are all temperature dependent, a factor of potential significance in electrophoresis. Therefore, extending the present system to take this factor into account is desirable in future study. Another problem of practical interest is to apply the present result to assess the stability (or critical coagulation concentration) of a colloidal dispersion, one of its key properties.

Acknowledgment

This work is supported by the National Science Council of the Republic of China.

Notation

Symbols

μ_E = electrophoretic mobility, m^2/V/s
ζ_P = zeta potential, V
ε = permittivity of the liquid phase, Coul^2/N/m^2
η = fluid viscosity, kg/m/s
κ = reciprocal Debye length, 1/m
a = radius of a rigid sphere, m
κa = double-layer thickness
E = strength of electric field, V/m
$N_{\equiv\text{M-OH}_2^+}$ = surface density of $\equiv \text{M-OH}_2^+$, no./m^2
$N_{\equiv\text{M-OH}}$ = surface density of $\equiv \text{M-OH}$, no./m^2
$N_{\equiv\text{M-O}^-}$ = surface density of $\equiv \text{M-O}$, no./m^2
N_{total} = total surface density of $\equiv \text{M-OH}$, no./m^2
$K_b = N_{\equiv\text{M-OH}_2^+}/N_{\equiv\text{M-OH}}[\text{H}^+]$, mol/m^3
$K_a = N_{\equiv\text{M-O}^-}[\text{H}^+]/N_{\equiv\text{M-OH}}$, mol/m^3
φ = electrical potential, V
ρ = space density of mobile ions, Coul/m^3
e = elementary charge, Coul
k_B = Boltzmann constant, J/K
T = absolute temperature, K
$\mathbf{u}$ = fluid velocity, m/s
p = pressure, Pa
z_j = valence of ionic species
n_j = number concentration of ionic species, no./m^3
$\mathbf{f}_j$ = flux of ionic species, no./s/m^2
D_j = diffusivity of ionic species, m^2/s
ζ_a = thermal potential, V
g_j = perturbed potential simulating the polarization of particle's double layer, V
σ_s = surface charge density, Coul/m^2
F = Faraday constant, Coul/mol
$\mathbf{e}_r$ = unit vector in the r direction
$\mathbf{n}$ = unit outer normal vector.

Abbreviations

PZC = point of zero charge
IEP = isoelectric point
MNPs = magnetic nanoparticles
DLS = dynamic light scattering

Literature Cited

1. Rakoczy R, Masiuk S. Influence of transverse rotating magnetic field on enhancement of solid dissolution process. *AIChE J*. 2010;56: 1416–1433.
2. Yang C, Guan Y, Xing J, Liu J, Shan G, An Z, Liu H. Preparation of magnetic polystyrene microspheres with a narrow size distribution. *AIChE J*. 2005;51:2011–2015.
3. Wei H, Wang E. Fe3O4 magnetic nanoparticles as peroxidase mimetics and their applications in H2O2 and glucose detection. *Anal Chem*. 2008;80:2250–2254.
4. Chang Q, Deng K, Zhu L, Jiang G, Yu C, Tang H. Determination of hydrogen peroxide with the aid of peroxidase-like Fe3O4 magnetic nanoparticles as the catalyst. *Microchim Acta*. 2009;165:299–305.
5. Moeser GD, Roach KA, Green WH, Hatton TA, Laibinis PE. High-gradient magnetic separation of coated magnetic nanoparticles. *AIChE J*. 2004;50:2835–2848.
6. Lee N, Hyeon T. Designed synthesis of uniformly sized iron oxide nanoparticles for efficient magnetic resonance imaging contrast agents. *Chem Soc Rev*. 2012;41:2575–2589.
7. Chomoucka J, Drbohlavova J, Huska D, Adam V, Kizek R, Hubalek J. Magnetic nanoparticles and targeted drug delivering. *Pharmacol Res*. 2010;62:144–149.
8. Li WL, Tang H, Zhang T, Li Q, Xing JM, Liu HZ. Ultra-deep desulfurization adsorbents for hydrotreated diesel with magnetic mesoporous aluminosilicates. *AIChE J*. 2010;56:1391–1396.
9. Zhang J, Zhuang J, Gao L, Zhang Y, Gu N, Feng J, Yang D, Zhu J, Yan X. Decomposing phenol by the hidden talent of ferromagnetic nanoparticles. *Chemosphere*. 2008;73:1524–1528.
10. Zhang S, Zhao X, Niu H, Shi Y, Cai Y, Jiang G. Superparamagnetic Fe_3O_4 nanoparticles as catalysts for the catalytic oxidation of phenolic and aniline compounds. *J Hazard Mater*. 2009;167:560–566.
11. Wang N, Zhu L, Wang M, Wang D, Tang H. Sono-enhanced degradation of dye pollutants with the use of H_2O_2 activated by Fe_3O_4 magnetic nanoparticles as peroxidase mimetic. *Ultrason Sonochem*. 2010;17:78–83.
12. Xie J, Xu C, Xu Z, Hou Y, Young KL, Wang SX, Pourmand N, Sun S. Linking hydrophilic macromolecules to monodisperse magnetite (Fe_3O_4) nanoparticles via trichloro-s-triazine. *Chem Mater*. 2006; 18:5401–5403.
13. Zhao X, Cai Y, Wang T, Shi Y, Jiang G. Preparation of alkanethiolate-functionalized core/shell Fe_3O_4@Au nanoparticles and its interaction with several typical target molecules. *Anal Chem*. 2008;80:9091–9096.
14. Zhang Y, Yang M, Portney NG, Cui D, Budak G, Ozbay E, Ozkan M, Ozkan CS. Zeta potential: a surface electrical characteristic to probe the interaction of nanoparticles with normal and cancer human breast epithelial cells. *Biomed Microdevices*. 2008;10:321–328.
15. Xie J, Xu C, Kohler N, Hou Y, Sun S. Controlled PEGylation of monodisperse Fe_3O_4 nanoparticles for reduced non-specific uptake by macrophage cells. *Adv Mater*. 2007;19:3163–3166.
16. Wang M, Wang N, Tang H, Cao M, She Y, Zhu L. Surface modification of nano-Fe_3O_4 with EDTA and its use in H2O2 activation for removing organic pollutants. *Catal Sci Technol*. 2012;2:187–194.
17. Illés E, Tombácz E. The role of variable surface charge and surface complexation in the adsorption of humic acid on magnetite. *Colloids Surf A*. 2004;230:99–109.
18. Goldberg S, Sposito G. A chemical model of phosphate adsorption by soils: I. reference oxide minerals. *Soil Sci Soc Am J*. 1984;48:772–783.
19. Tamura H, Katayama N, Furuich R. Modeling of ion-exchange reactions on metal oxides with the Frumkin isotherm. 1. Acid-base and charge characteristics of MnO_2, TiO_2, Fe_3O_4, and Al_2O_3 surfaces and adsorption affinity of alkali metal ions. *Environ Sci Technol*. 1996;30:1198–1204.
20. Kosmulski M. Compilation of PZC and IEP of sparingly soluble metal oxides and hydroxides from literature. *Adv Colloid Interface Sci*. 2009;152:14–25.
21. Huang SH, Chen DH. Rapid removal of heavy metal cations and anions from aqueous solutions by an amino-functionalized magnetic nano-adsorbent. *J Hazard Mater*. 2009;163:1174–1179.
22. Wang SH, Shi X, Antwerp MV, Cao Z, Swanson SD, Bi X, Baker JR. Dendrimer-functionalized iron oxide nanoparticles for specific targeting and imaging of cancer cells. *Adv Funct Mater*. 2007;17:3043–3050.
23. Smoluchowski MV. Mathematical theory of the kinetics of the coagulation of colloidal solutions. *Z Phys Chem*. 1918;92:129–168.
24. Hückel E. The cataphoresis of the sphere. *Phys Z*. 1924;25:204–210.
25. Henry DC. The cataphoresis of suspended particles, Part I. The equation of cataphoresis. Proc R. Soc London A. 1931;133:106–129.
26. Hsu JP, Chen ZS. Electrophoresis of a sphere along the axis of a cylindrical pore: effects of double-layer polarization and electroosmotic flow. *Langmuir*. 2007;23:6198–6204.
27. Yeh LH, Hsu JP. Effects of double-layer polarization and counterion condensation on the electrophoresis of polyelectrolytes. *Soft Matter*. 2011;7:396–411.
28. Hsu JP, Huang CH, Tseng S. Gel electrophoresis: importance of concentration-dependent permittivity and double-layer polarization. *Chem Eng Sci*. 2012;84:574–579.
29. O'Brien RW, White LR. Electrophoretic mobility of a spherical colloidal particle. *J Chem Soc Faraday Trans 2*. 1978;74:1607–1626.
30. Leroy P, Revil A. A triple-layer model of the surface electrochemical properties of clay minerals. *J Colloid Interface Sci*. 2004;270:371–380.
31. Bowden JW, Posner AM, Quirk JP. Ionic adsorption on variable charge mineral surfaces. Theoretical charge development and titration curves. *Aust J Soil Res*. 1977;15:121–136.
32. Sonnefeld J, Lobbus M, Vogelsberger W. Determination of electric double layer parameters for spherical silica particles under application of the triple layer model using surface charge density data and results of electrokinetic sonic amplitude measurements. *Colloids Surf A*. 2001;195:215–225.
33. Qian S, Wang A, Afonien JK. Electrophoretic motion of a spherical particle in a converging-diverging nanotube. *J Colloid Interface Sci*. 2006;303:579–592.
34. Ohshima H. Electrophoresis of soft particles. *Adv Colloid Interface Sci*. 1995;62:189–235.
35. Ohshima H. Electrophoresis of soft particles: analytic approximations. *Electrophoresis*. 2006;27:526–533.
36. Hsu JP, Yeh LH, Ku MH. Evaluation of the electric force in electrophoresis. *J Colloid Interface Sci*. 2007;305:324–329.
37. Kampmeyer PM. The temperature dependence of viscosity for water and mercury. *J Appl Phys*. 1952;23:99–102.
38. Owen BB, Milner CE, Miller RC, Cogan HL. Dielectric constant of water as a function of temperature and pressure. *J Phys Chem*. 1961; 65:2065–2070.
39. Poling BE, Prausnitz JM, O'Connell JP. The Properties of Gases and Liquids, 5th ed. New York: McGraw-Hill, 2001.
40. Stewart PA. How to Understand Acid-Base. New York: Elsevier, 1981.
41. Wang N, Zhu L, Wang D, Wang M, Lin Z, Tang H. Sono-assisted preparation of highly-efficient peroxidase-like Fe_3O_4 magnetic nanoparticles for catalytic removal of organic pollutants with H_2O_2. *Ultrason Sonochem*. 2010;17:526–533.
42. Wang N, Hsu C, Zhu L, Tseng S, Hsu JP. Influence of metal oxide nanoparticles concentration on their zeta potential. *J Colloid Interface Sci*. 2013;407:22–28.
43. Xue XF, Hanna K, Despas C, Wu F, Deng NS. Effect of chelating agent on the oxidation rate of PCP in the magnetite/H_2O_2 system at neutral pH. *J Mol Catal A: Chem*. 2009;311:29–35.
44. Hsu JP, Tai YH, Yeh LH. Importance of temperature effect on the electrophoretic behavior of charge-regulated particles. *Langmuir*. 2012;28:1013–1019.
45. Hsu JP, Yee CP, Yeh LH. Importance of electroosmotic flow and multiple ionic species on the electrophoresis of a rigid sphere in a charge-regulated zwitterionic cylindrical pore. *Langmuir*. 2012;28: 10942–10947.
46. Hsu JP, Tai YH. Effect of multiple ionic species on the electrophoretic behavior of a charge-regulated particle. *Langmuir*. 2010;26:16857–16864.
47. Missana T, Adell A. On the applicability of DLVO theory to the prediction of clay colloids stability. *J Colloid Interface Sci*. 2000;230:150–156.
48. Volkov AG, Paula S, Deamer DW. Two mechanisms of permeation of small neutral molecules and hydrated ions across phospholipid bilayers. *Bioelectrochem Bioenerg*. 1997;42:153–160.

Manuscript received Jun. 10, 2013, and revision received Sept. 11, 2013.